Light particle emission in ^{16}O-induced reactions on ^{12}C, ^{27}Al, and ^{197}Au at $E/A = 25$ MeV

C. B. Chitwood, D. J. Fields, C. K. Gelbke, D. R. Klesch,* W. G. Lynch, and M. B. Tsang
National Superconducting Cyclotron Laboratory, Michigan State University, East Lansing, Michigan 48824

T. C. Awes, R. L. Ferguson, F. E. Obenshain, F. Plasil, R. L. Robinson, and G. R. Young
Physics Division, Oak Ridge National Laboratory, Oak Ridge, Tennessee 37831
(Received 26 March 1986)

Single- and two-particle inclusive cross sections of light particles (p,d,t) were measured for ^{16}O-induced reactions on ^{12}C, ^{27}Al, and ^{197}Au at $E/A = 25$ MeV. The energy and angular distributions indicate that these particles originate from violently interacting subsets of the projectile-target system. For reactions on ^{197}Au, the two-particle correlations at large relative momenta indicate an ordered motion in the entrance channel reaction plane which is superimposed on the random velocities of the constituents of these subsets. For reactions on ^{12}C, the two-particle correlations appear to be dominated by momentum and energy conservation.

I. INTRODUCTION

At incident energies of only a few MeV per nucleon above the interaction barrier, nucleus-nucleus collisions are dominated by mean field effects and one body dissipation.[1] With the exception of very heavy systems, collisions at small impact parameters are understood in terms of the complete fusion of projectile and target, the formation of a fully equilibrated compound nucleus, and its subsequent statistical decay by particle and γ-ray emission.[2-4] As the projectile energy is increased to a few tens of MeV per nucleon above the barrier, two-body dissipation becomes increasingly important. In this energy range, central collisions are characterized by incomplete fusion and particle emission prior to the attainment of full statistical equilibrium in the composite system.[5-15] Detailed investigations of noncompound light particle emission provide information about the dynamical and statistical aspects of these reactions at the early stages of the projectile and target interaction.[16]

Single particle inclusive cross sections for the emission of noncompound light particles have been described rather successfully in terms of simple Maxwellian energy distributions centered at velocities slightly less than half the beam velocity.[9,10,14] For ^{16}O induced reactions on ^{238}U at $E/A \approx 20$ MeV, the emission of noncompound light particles was shown[9] to be dominated by violent projectile-target interactions in which the major part of the projectile is absorbed by the target nucleus; the average multiplicity of noncompound light particles was shown to be of the order of 1. The successful description of noncompound light particle emission in terms of simple Maxwellian distributions (moving source parametrizations) cannot,[9,10] therefore, be interpreted in terms of particle emission from a hot source of nucleons which is separated from the target nucleus. However, such parametrizations indicate that the light particle velocities are randomized in rest frames different from the compound nucleus rest frame.

Present experimental information is consistent with the concept of statistical particle emission from highly excited subsets of nucleons which are in the process of equilibration with the remaining composite system. However, little is known about the relative importance of dynamical and statistical aspects of the reactions which should reflect the interplay of the collective motion in the mean nuclear field and the randomization of the particle velocities by individual nucleon-nucleon collisions. The relative importance of these effects is expected to change dramatically in the transition energy regime where the relative velocity between projectile and target nuclei is of a magnitude comparable to the Fermi velocity.

In order to obtain further information about the dynamical and statistical aspects of nuclear reactions in the transition energy regime of a few tens of MeV per nucleon, we have measured correlations between two coincident light particles emitted with large relative momenta in ^{16}O induced reactions on ^{12}C and ^{197}Au targets at $E/A = 25$ MeV. At large relative momenta, final state interactions between the coincident particles are expected to be negligible. The correlations should, therefore, be sensitive to geometrical and dynamical aspects of the reaction which cannot be extracted from single particle inclusive measurements. The comparison of two-particle correlations measured for reactions on a heavy and a light target nucleus is expected to provide useful information about the importance of finite particle effects (e.g., phase space constraints for small ensembles due to conservation laws), collective flow effects, and possible shadowing effects. A brief report of these correlation measurements has been published previously.[17] In order to obtain more systematic information about the energy and target dependence of noncompound light particle emission, we have also performed single particle inclusive measurements of high statistical accuracy. These data were fitted with several versions of a single moving source parametrization to determine the stability and sensitivity of the parameters.

This paper is organized as follows: Details of the experimental setup and data reduction are given in Sec. II. In Sec. III the single-particle inclusive cross sections are

presented and discussed in terms of several simple parametrizations. Associated light particle multiplicities are presented in Sec. IV. In Sec. V two-particle correlations at large relative momenta are discussed and shown to be sensitive to both reaction dynamics and phase-space constraints. Our summary and conclusions are given in Sec. VI.

II. EXPERIMENTAL DETAILS

The experiment was performed at the Holifield Heavy-Ion Research Facility of Oak Ridge National Laboratory. ^{12}C, ^{27}Al, and ^{197}Au targets of 2.4, 3.0, and 9.7 mg/cm^2 areal density, respectively, were bombarded with ^{16}O ions of 400 MeV incident energy. A schematic drawing of the experimental setup is given in Fig. 1. Single- and two-light-particle inclusive cross sections were measured with thirteen ΔE-E telescopes consisting of silicon ΔE and NaI E detectors. Correlations at small relative momenta were measured with six telescopes mounted in a closely packed hexagonal array that was centered at angles $\theta=15°$ and $\phi=180°$, where θ and ϕ denote the polar and azimuthal angles measured with respect to the beam axis. These correlations were published previously[18–20] and will not be discussed in this paper. Correlations at large relative momenta were measured with an additional seven telescopes of solid angles between 13 and 40 msr. Three of these telescopes were mounted at the fixed azimuthal angle of $\phi=0°$ and at the polar angles of $\theta=40°$, 70°, and 130°. The remaining four telescopes were positioned at the polar angles of $\theta=40°$, 70°, 130°, and 160°; their common azimuthal angle was varied between 50° and 180°. In order to protect the detectors from excessive radiation damage, heavy recoil nuclei and fission fragments were stopped in 0.22 mm thick Al foils placed in front of the Si detectors. The absolute normalization of the cross sections is accurate to 10%. Energy calibrations, accurate to 3%, were obtained by measuring the energies of recoil protons backscattered from a Mylar target by a 200-MeV ^{16}O beam.

In order to detect and correct for gain shifts of the NaI detectors, the following procedure was developed for the off-line analysis. For each run the raw data were sorted into two-dimensional ΔE-E matrices. Since the calibration of the Si detectors did not change appreciably during the experiment, several narrow gates were set on the ΔE signals. The events which fell into these gates were projected onto the E axis. Each of the peaks corresponding to different particles was then fitted with a Gaussian function to determine the peak location, C_i. The relative gain shift for each run with respect to the calibration run was then determined for each detector by minimizing the function $\chi^2(x)$,

$$\chi^2(x)=\sum_i (xC_i-C_{0i})^2/C_{0i}^2 , \tag{1}$$

with respect to the gain shift parameter x. Here, the centroids determined for the calibration run are denoted by C_{0i}. With this procedure, gain shifts of the order of 1% could be detected and corrected.

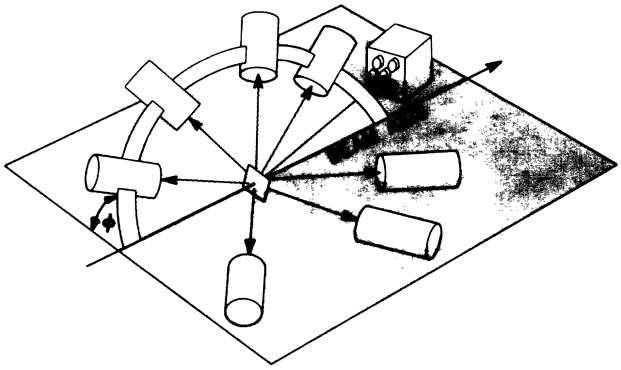

FIG. 1. Schematic diagram of the experimental setup.

III. SINGLE PARTICLE INCLUSIVE SPECTRA

Double differential cross sections of light particles emitted in reactions induced by ^{16}O ions of 400 MeV incident energy on targets of ^{12}C, ^{27}Al, and ^{197}Au are presented in Figs. 2–4. The energy spectra exhibit smooth exponential slopes which become steeper with increasing detection angle; they are similar to those measured for reactions with a wide range of energies and projectile-target combinations.[5–16]

In order to compare our data with the systematic trends established in previous experiments, we fit the spectra with a single Maxwellian distribution centered at a velocity v_0. Nonrelativistic kinematics[21] were used to calculate the cross sections in the laboratory rest frame according to

$$\frac{d^2\sigma}{dE\,d\Omega}=N_0(E-V_c)^{1/2}\exp(-E_s/T) , \tag{2}$$

with

$$E_s=E-V_c+E_0-2[E_0(E-V_c)]^{1/2}\cos\theta . \tag{3}$$

Here, N_0 is a normalization constant, E and m are the energy and mass of the emitted particle, θ is the detection angle, T is the source "temperature," $E_0=mv_0^2/2$, and V_c corrects for the Coulomb repulsion from the target residue.[9,22]

The low energy portions of the energy spectra are expected to have significant contributions from the later, more equilibrated stages of the reaction for which the present parametrization should be inadequate. We, therefore, have only fitted the high energy portions of the energy spectra. For protons, only energies above 15 MeV were included in the fits; for deuterons and tritons only energies above 20 MeV were included. The Coulomb correction V_c was fixed at 3, 4, and 10 MeV for the ^{12}C, ^{27}Al, and ^{197}Au targets, respectively. The overall fits obtained with the "moving source" parametrization of Eq. (2) are shown by dotted-dashed lines in Figs. 2–4. The fit parameters are listed in Table I. Similar source velocities are extracted from the energy spectra of protons, deuterons, and tritons. For reactions on ^{27}Al and ^{197}Au, these velocities are slightly less than half the beam velocity, but considerably larger than the compound nucleus velocity, indicating particle emission prior to the attainment of full

statistical equilibrium in the composite system. For reactions on ^{12}C, however, the source velocities are slightly less than the compound nucleus velocity, $v_{CN}=0.13c$. For nearly symmetric systems, noncompound light particle emission is not separated kinematically from emission by the fully equilibrated composite system.[10] Slightly larger values of T are extracted for heavier hydrogen isotopes. At intermediate angles, the simple moving source parametrization provides a reasonable description of the data. However, the parametrization does not describe the cross sections at forward and backward angles.[10] At these angles, statistical emission from fully equilibrated projectile and target residues may be important, and a description in terms of emission from an intermediate rapidity source is indaequate.

The temperature parameters determined from the present set of data follow the smooth dependence on the projectile velocity established for similar reactions over a wide range of incident energies,[10,14,16] as shown in Fig. 5. The solid line in the figure is drawn to guide the eye. For orientation, the dotted-dashed line shows the energy dependence of the temperature of an ideal Fermi gas at normal nuclear density, $\rho=\rho_0$, which is composed of equal numbers of projectile and target nucleons.[10] The dashed line corresponds to calculations[14] for a free, strongly interacting gas in thermal and chemical equilibrium as predicted by the fireball model[23,24] for the impact parameter of maximum weight, assuming a freeze-out density of $\rho_f=\rho_0$. Also included in this figure are the "slope parameters" extracted[25] from the energy spectra of neutral pions emitted in the reactions $^{12}C+^{238}U$ and $^{12}C+^{12}C$. It is interesting that these slope parameters follow similar systematics.

The description of the inclusive spectra in terms of Eq.

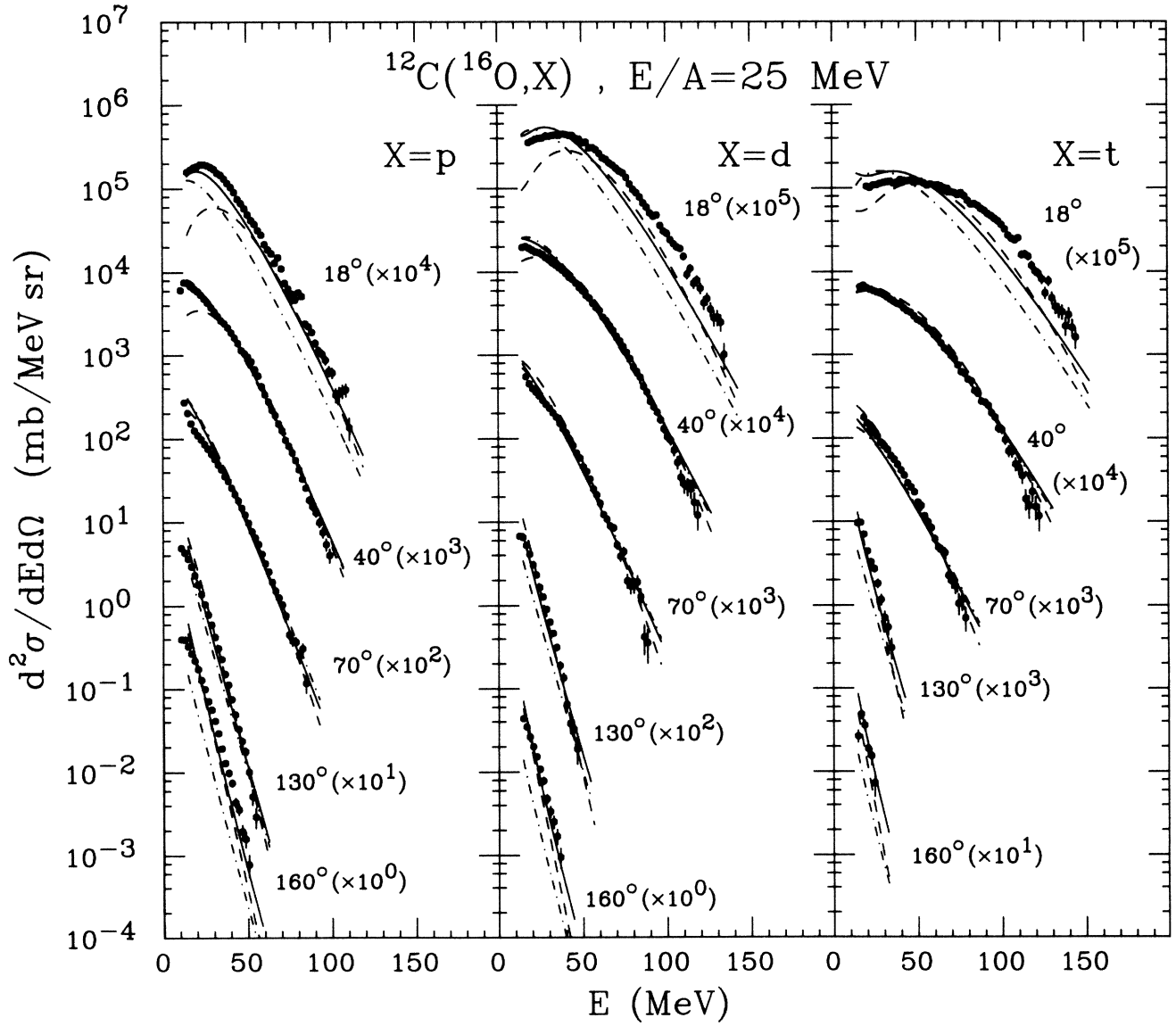

FIG. 2. Single particle inclusive proton, deuteron, and triton cross sections for ^{16}O induced reactions on ^{12}C at $E/A=25$ MeV. The dotted-dashed lines represent fits with Eq. (2); the solid and dashed lines represent fits with Eqs. (4) and (5), respectively. See text for more details.

(2) is not ideal. Furthermore, the assumption of azimuthally symmetric particle emission implicit in Eq. (2) is at variance with recent experimental results[17,26] which indicate that noncompound light particles are preferentially emitted in a plane which contains the beam axis (see also Sec. V). In the extreme limit of isotropic particle emission in such a plane, $d\sigma/d\theta=$const; the single particle cross sections (averaged over the azimuthal orientation of this plane) are given by $d\sigma/d\Omega \propto 1/\sin\theta$. Assuming Maxwellian energy distributions centered around a velocity v_0, one obtains, in the laboratory rest frame,

$$\frac{d^2\sigma}{dE\,d\Omega}=\frac{N_0 E_s^{1/2}}{\sin\theta}\exp(-E_s/T)\,, \tag{4}$$

where E_s is given by Eq. (3). The solid curves in Figs. 2–4 show fits with this parametrization. The parameters are listed in Table I; they are similar to those obtained with the isotropic Maxwellian distribution. Equation (4) gives, however, a significantly better description of the singles data. The improvement is particularly striking at more forward angles.

Previous measurements have shown that the preferential emission of nonequilibrium light particles in the entrance channel reaction plane becomes more pronounced with increasing mass of the emitted particles.[26] This effect can be understood in terms of an ordered motion in the reaction plane which is superimposed on the random velocities of the emitted particles.[17,26] Microscopically, these aspects can be understood in terms of the macroscopic flow mediated by the mean field and the random velocities caused by the combined effects of nucleon-nucleon collisions and Fermi motion.[27] Since the assump-

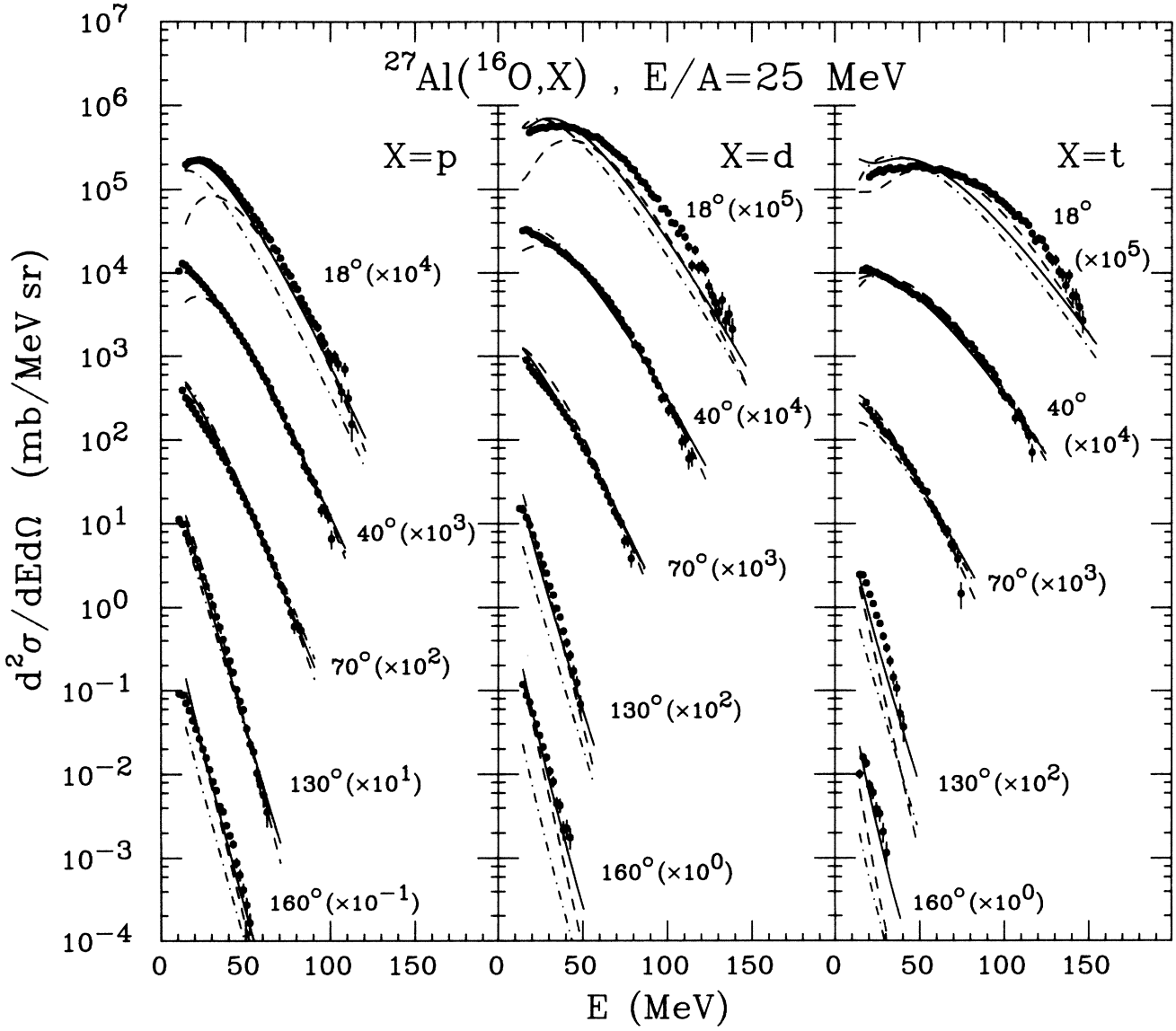

FIG. 3. Single particle inclusive proton, deuteron, and triton cross sections for ^{16}O induced reactions on ^{27}Al at $E/A=25$ MeV. The dotted-dashed lines represent fits with Eq. (2); the solid and dashed lines represent fits with Eqs. (4) and (5), respectively. See text for more details.

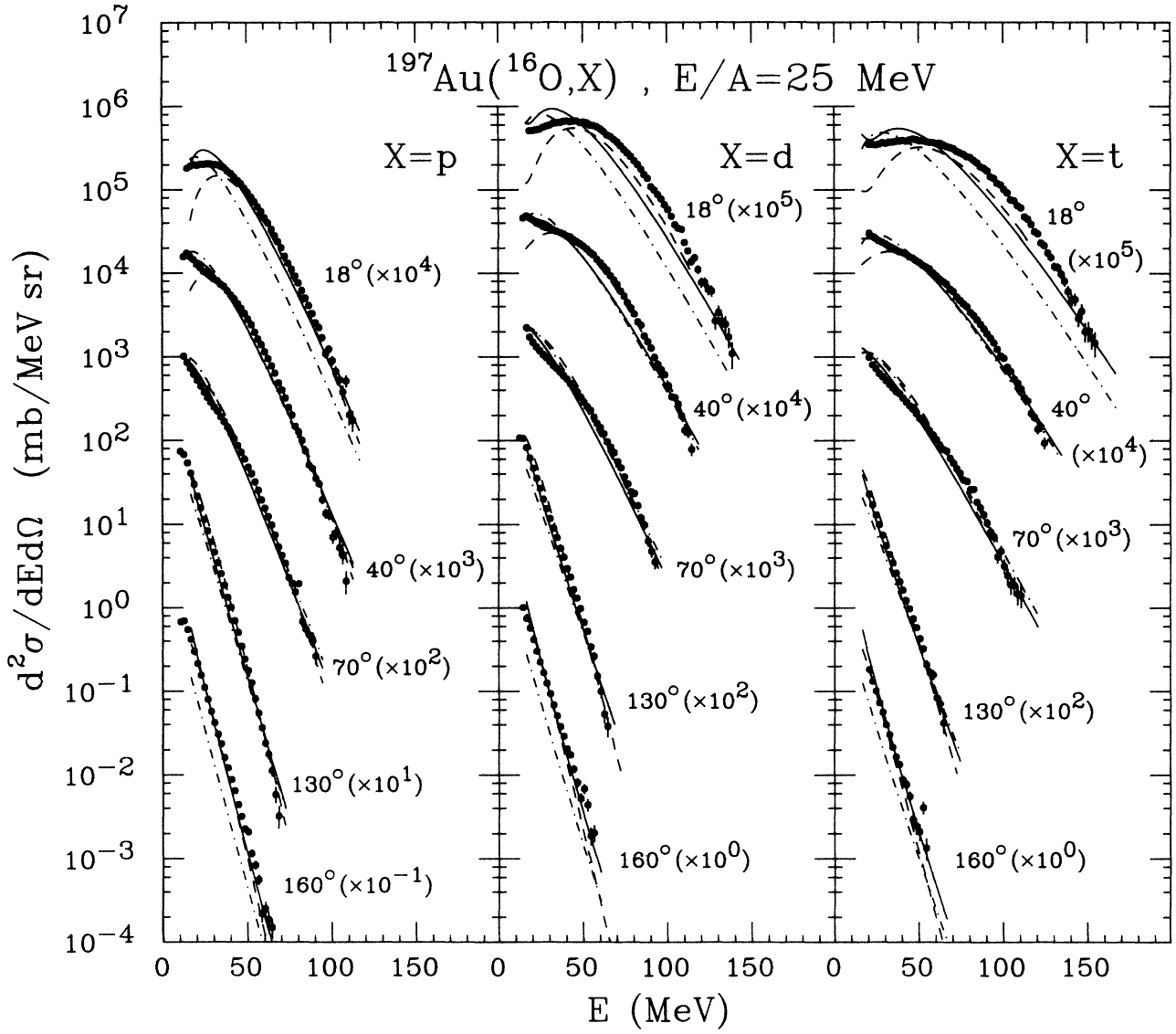

FIG. 4. Single particle inclusive proton, deuteron, and triton cross sections for ^{16}O induced reactions on ^{197}Au at $E/A=25$ MeV. The dotted-dashed lines represent fits with Eq. (2); the solid and dashed lines represent fits with Eqs. (4) and (5), respectively. See text for more details.

tion of strictly coplanar emission is unrealistic, we have employed an alternative parametrization to illustrate the interplay of random and collective velocity components. For a rotating ideal gas of temperature T, one has[28]

$$\frac{d^2\sigma}{dE\,d\Omega}(E,\theta,\phi)=N_0[(E-V_c)E_s]^{1/2}\exp(-E_s/T)\frac{J_1(iK)}{iK}, \tag{5}$$

where E_s is given by Eq. (3) and

$$K=\frac{R\omega}{T}\{2m[E_s-(E-V_c)\sin^2\theta\sin^2\phi]\}^{1/2}. \tag{6}$$

Here, J_1 denotes the first-order Bessel function, and θ and ϕ are the polar and azimuthal angles of the emitted particle. In our convention, the polar and azimuthal angles of the angular velocity vector ω are $\theta_\omega=90°$ and $\phi_\omega=90°$, respectively. A brief derivation[28] of Eq. (5) is given in the Appendix. (This equation will also be used in the discussion of the two-particle correlation function; see Sec. V.) Single particle distributions are obtained after averaging over the azimuthal angle ϕ. The dashed lines in Figs. 2–4 show fits to the singles data with Eq. (5); the parameters are listed in Table I. The overall quality of the fits is satisfactory. The temperature parameters T are consistently lower than those extracted from the previous parametrizations. In part, this effect is due to the additional factor of $E_s^{1/2}$ which can be traced back[29] to the assumption of emission from the surface; see the derivation given in the Appendix. Equations (2) and (4), on the other hand, correspond to volume emission.[29] To a large extent, however, the low temperatures extracted with Eq. (5) are due to the collective rotation which tends to make the slopes of the energy spectra less steep. [Note that $J_1(iK)/iK$ is a monotonically increasing function for $K>0$.] The use of Eq. (5) illustrates the difficulties of extracting unambigu-

TABLE I. Parameters used for the calculations shown in Figs. 2–4.

Target	Eq.	Particle	v_0/c	T (MeV)	σ_0 (b)	$R\omega/c$
^{197}Au	(2)	p	0.095	7.17	2.18±0.05	
		d	0.093	8.73	0.77±0.02	
		t	0.089	9.93	0.50±0.01	
^{197}Au	(4)	p	0.098	7.15	2.73±0.06	
		d	0.097	8.64	1.02±0.02	
		t	0.095	9.74	0.67±0.01	
^{197}Au	(5)	p	0.094	4.20	1.19±0.06	0.129
		d	0.095	4.67	0.74±0.04	0.104
		t	0.093	5.56	0.47±0.02	0.086
^{27}Al	(2)	p	0.110	7.63	1.49±0.04	
		d	0.123	8.34	0.542±0.014	
		t	0.129	9.09	0.194±0.004	
^{27}Al	(4)	p	0.114	7.53	2.01±0.05	
		d	0.116	8.51	0.760±0.018	
		t	0.123	9.30	0.277±0.006	
^{27}Al	(5)	p	0.110	4.59	1.07±0.08	0.131
		d	0.113	4.80	0.49±0.03	0.099
		t	0.126	4.98	0.215±0.01	0.080
^{12}C	(2)	p	0.116	7.25	1.02±0.03	
		d	0.116	7.86	0.38±0.01	
		t	0.118	8.61	0.121±0.003	
^{12}C	(4)	p	0.117	7.12	1.46±0.04	
		d	0.117	7.86	0.54±0.01	
		t	0.119	8.60	0.173±0.004	
^{12}C	(5)	p	0.114	4.22	0.72±0.06	0.134
		d	0.114	4.36	0.337±0.02	0.099
		t	0.116	4.67	0.132±0.007	0.089

ous temperature parameters if the effects of collective motion are unknown.[30]

Fits of single particle cross sections with the simple parametrization of Eqs. (2), (4), and (5) were used to extract the cross sections which may be associated with the emission from a thermalized source at intermediate rapidity.[14,31,32] Of particular physical interest are relative particle production cross sections which may provide key information concerning the entropy production in nuclear collision experiments.[32–34] In order to assess the uncertanties of the intermediate rapidity cross sections which have to be associated with the use of different parametrizations of the single particle inclusive cross sections, the calculated energy and angle integrated cross sections,

$$\sigma_0 = \int dE\, d\Omega (d^2\sigma/dE\, d\Omega) ,$$

corresponding to the different fits are listed in Table I. The corresponding particle production ratios are compared in Table II. The absolute magnitudes of the extracted cross sections can differ by 30–50%. However, the extracted particle production ratios are less sensitive to the particular choice of parametrization. For reactions on ^{197}Au, rather low abundances of deuterons and tritons as compared to protons are extracted: $\sigma_d/\sigma_p = 0.38 \pm 0.03$,

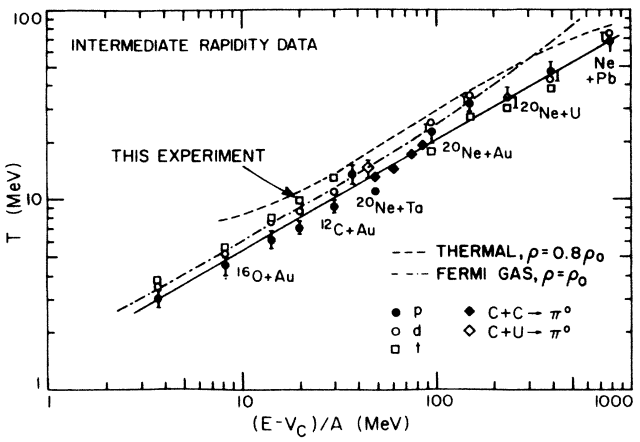

FIG. 5. Dependence of temperature parameters on projectile energy per nucleon above the Coulomb barrier obtained by fitting intermediate rapidity, single particle inclusive cross sections with the moving source parametrization (Refs. 10 and 14) (at higher energies relativistic transformations to the laboratory frame are used). The diamond shaped symbols correspond to temperature parameters extracted from neutral pion measurements (Ref. 25).

TABLE II. Light particle cross section ratios extracted from fits to the data.

Target	Ratio	Eq. (2)	Eq. (4)	Eq. (5)
^{197}Au	σ_d/σ_p	0.353	0.375	0.411
^{197}Au	σ_t/σ_p	0.229	0.246	0.262
^{27}Al	σ_d/σ_p	0.364	0.378	0.457
^{27}Al	σ_t/σ_p	0.130	0.138	0.200
^{12}C	σ_d/σ_p	0.373	0.369	0.467
^{12}C	σ_t/σ_p	0.119	0.118	0.183

$\sigma_t/\sigma_p=0.24\pm0.02$. These values are consistent with those reported[14,32] for a large range of energies and projectile target combinations. These low composite particle abundances have been associated with unusually high entropy values,[31–33] which are difficult to understand with existing models.[34]

IV. ASSOCIATED MULTIPLICITIES

The integrated cross sections extracted for the emission of noncompound light particles are of the order of a few barns, i.e., they are comparable to the reaction cross section (see Table I). The average number of noncompound light particles per nuclear collision is, therefore, of the order of unity. More quantitative information may be gained from the associated multiplicity, $M_2(\theta_1,\Delta E_1,\Delta E_2)$, which is defined as the multiplicity of particle 2, integrated over all angles and over the energy interval ΔE_2, emitted in coincidence with a "trigger" particle 1 detected at the angle θ_1 and of outgoing energy in the interval ΔE_1:

$$M_2(\theta_1,\Delta E_1,\Delta E_2) = \frac{\int_{\Delta E_2} dE_2 d\Omega_2 \int_{\Delta E_1} dE_1 \frac{d^4\sigma_{12}}{dE_1 d\Omega_1 dE_2 d\Omega_2}}{\int_{\Delta E_1} dE_1 \frac{d^2\sigma_1}{dE_1 d\Omega_1}} . \quad (7)$$

Figure 6 shows the associated light particle multiplicities measured for reactions on ^{197}Au. The energy integrations were performed over the energy intervals of $\Delta E_1=20$–80 MeV and $\Delta E_2=20$–80 MeV. Within the experimental uncertainties, the associated multiplicities are independent of the choice of trigger particle 1; no significant dependence on the emission angle of the trigger particle is observed. For protons, deuterons, and tritons, the average associated multiplicities are $M_p=0.38$, $M_d\approx0.17$, and $M_t\approx0.12$, respectively. Coincidence cross sections at angles forward of 15° were not measured in this experiment. If the coincidence cross sections would rise significantly at these small angles, the associated multiplicities would be slightly larger.

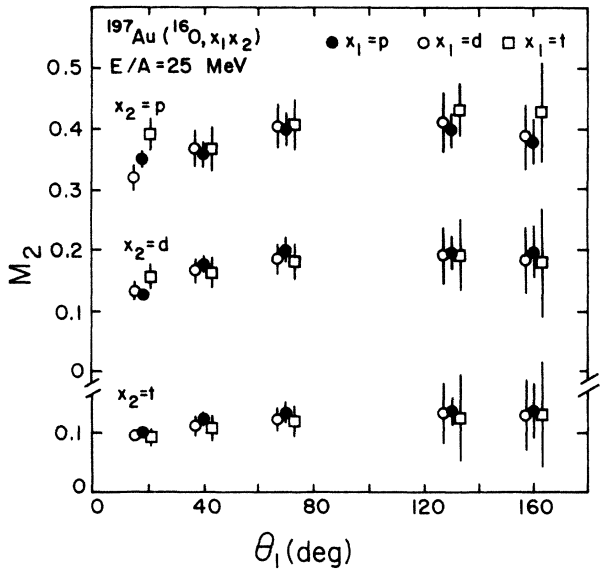

FIG. 6. Associated multiplicities, defined in Eq. (7), for the emission of noncompound light particles, x_1 and x_2, emitted in ^{16}O induced reactions on ^{197}Au at $E/A=25$ MeV. The trigger particle is denoted x_1. The energies of particles 1 and 2 were integrated over the energy intervals of $\Delta E_1=20$–80 MeV and $\Delta E_2=20$–80 MeV, respectively.

It was already pointed out in Refs. 9 and 10 that the description of single particle inclusive cross sections in terms of various "moving source parametrizations" could not be interpreted in terms of particle emission from a hot gas of nucleons which is separated from the target nucleus. Such parametrizations merely indicate that the light particle velocities are randomized in rest frames different from the compound nucleus rest frame. The small associated light particle multiplicities measured in this experiment corroborate this point: at energies of only a few tens of MeV, a free nuclear fireball[23,24] does not exist.

V. TWO-PARTICLE CORRELATIONS AT LARGE RELATIVE MOMENTA

In order to eliminate the strong dependence of the single particle distributions on angle and energy of the emitted particles, and to be sensitive to the dynamical aspects of the reaction, we present our coincidence data in terms of the two-particle correlation function $C(\theta_1,\theta_2,\phi)$ which is defined as[35]

$$C(\theta_1,\theta_2,\phi) = \frac{\int_{\Delta E_1} dE_1 \int_{\Delta E_2} dE_2 \frac{d^4\sigma_{12}}{dE_1 d\Omega_1 dE_2 d\Omega_2}(E_1,E_2,\theta_1,\theta_2,\phi)}{\int_{\Delta E_1} dE_1 \frac{d^2\sigma_1}{dE_1 d\Omega_1}(E_1,\theta_1) \int_{\Delta E_2} dE_2 \frac{d^2\sigma_2}{dE_2 d\Omega_2}(E_2,\theta_2)} , \quad (8)$$

where θ_1 and θ_2 denote the polar angles of particles 1 and 2, and ϕ is the difference of the azimuthal angles with respect to the beam axis; see Fig. 7 for the definition of these angles. For the case of uncorrelated emission, $C(\theta_1,\theta_2,\phi)=$const, the two-particle cross sections are proportional to the product of the corresponding single particle cross sections.[36,37]

The two-particle correlation functions measured in this experiment are presented in Figs. 8–19. Low energies were excluded from these correlations in order to reduce contributions from the more equilibrated stages of the reaction.[17] The intervals ΔE_1 and ΔE_2 over which the energy integrations were performed are given in the figures. The upper and lower parts of the figures show correlations for $\theta_1=40°$ and 70°, respectively. The leftmost parts of the figures show correlations between particles detected in a common plane with the beam axis. For these correlations, relative azimuthal angles $\phi=0°$ are displayed as negative polar angles, $\theta_2<0$ (emission to the same side of the beam axis); positive polar angles, $\theta_2>0$, correspond to $\phi=180°$ (emission to opposite sides of the beam axis). The correlations at $\theta_2=15°$, 40°, and 70° are shown as a function of azimuthal angle, ϕ, in the three right-hand sections of these figures.

The correlations measured for the $^{16}O+^{12}C$ reaction are shown in Figs. 8–13. For all measured particle combinations, the correlation functions have maximum values if the two coincident particles are emitted in a plane which contains the beam axis. Emission of two particles to opposite sides of the beam axis is more likely than emission to the same side of the beam axis, i.e., the correlation functions have a maximum at $\phi=180°$. This enhanced emission to opposite sides of the beam axis becomes more pronounced for larger emission angles, θ_1 and θ_2, and for heavier particles.

Particle correlations are influenced by phase space constraints imposed by conservation laws.[17,35,38] This influence can dominate the correlations measured for small systems, such as the $^{16}O+^{12}C$ system. In order to demonstrate the effects of energy and momentum conservation, we have performed schematic calculations with a moving source parametrization which incorporates the effect of energy and momentum conservation.[35] In these calculations, the two particles were assumed to be emitted

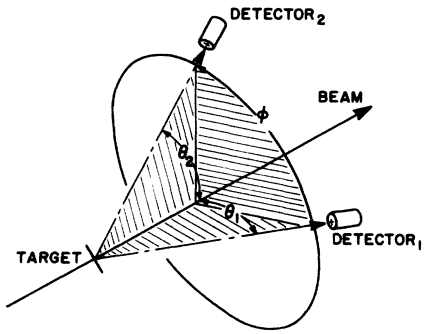

FIG. 7. Definition of angles θ_1, θ_2, and ϕ used for the presentation of the two-particle correlations; see also Eq. (8).

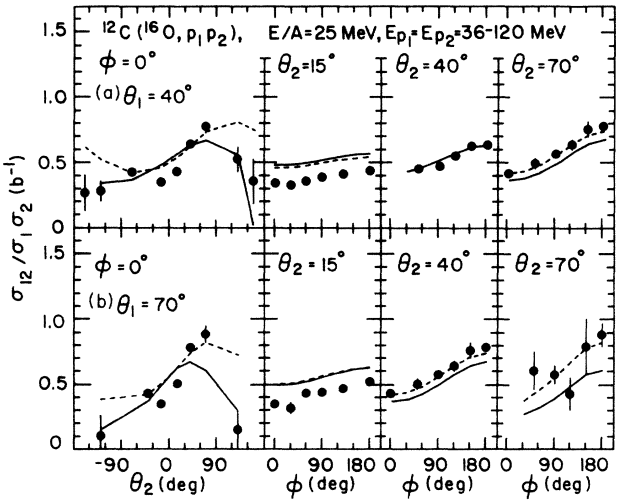

FIG. 8. Two-particle correlations between coincident protons emitted in ^{16}O induced reactions on ^{12}C at $E/A=25$ MeV. The solid and dashed lines are explained in the text.

sequentially. For the emission of the first particle, a Maxwellian velocity distribution of temperature $T=7.3$ MeV and mean velocity $v_0=0.13c$, directed parallel to the beam axis, was assumed. These parameters correspond to the compound nucleus velocity and temperature. For the emission of the second particle, a Maxwellian velocity distribution of temperature T' and mean velocity

$$\mathbf{v}_0'=(A_0\mathbf{v}_0-A_1\mathbf{v}_1)/(A_0-A_1)$$

was assumed. Here, $\mathbf{v}_1$ and A_1 denote the velocity and mass number of the first emitted particle, and $A_0=28$ is the mass number of the compound nucleus. Because of energy conservation, the excitation energy of the second source is reduced. We assumed, for the new temperature,

$$T'^2=E_x'(8\text{ MeV})/(A_0-A_1)\ ;$$

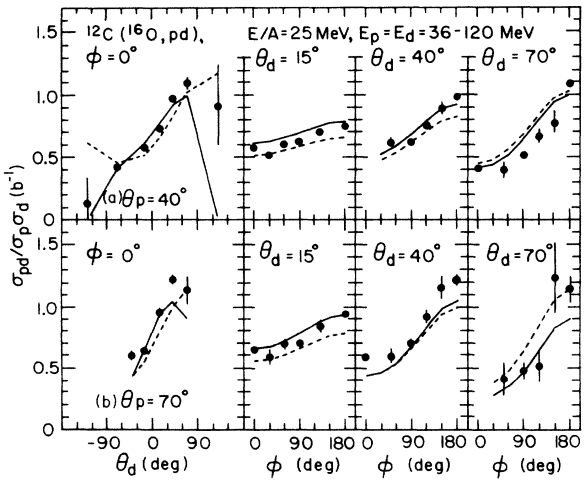

FIG. 9. Two-particle correlations between coincident protons and deuterons emitted in ^{16}O induced reactions on ^{12}C at $E/A=25$ MeV. The solid and dashed lines are explained in the text.

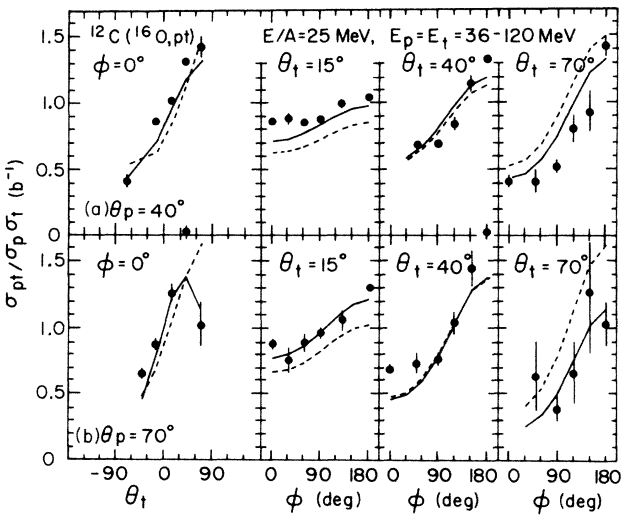

FIG. 10. Two-particle correlations between coincident protons and tritons emitted in ^{16}O induced reactions on ^{12}C at $E/A=25$ MeV. The solid and dashed lines are explained in the text.

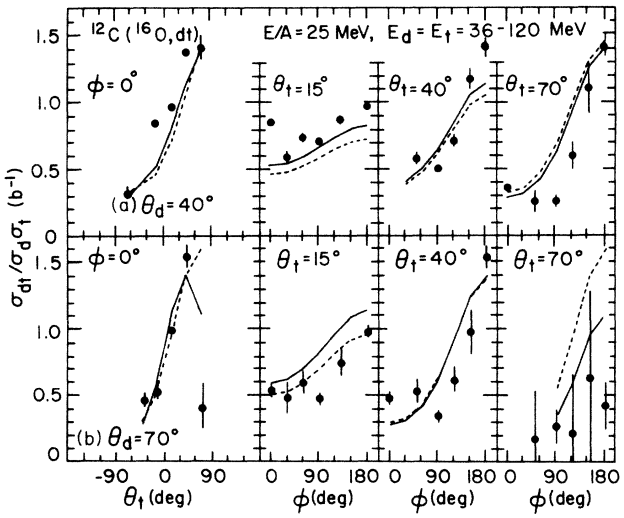

FIG. 12. Two-particle correlations between coincident deuterons and tritons emitted in ^{16}O induced reactions on ^{12}C at $E/A=25$ MeV. The solid and dashed lines are explained in the text.

here,

$$E_x - E_x' = \frac{m_0}{2}(\mathbf{v}_1 - \mathbf{v}_0)^2 A_1 A_0/(A_0 - A_1)\,,$$

$$E_x = A_0 T^2/(8\ \text{MeV})\,,$$

and m_0 denotes the nucleon mass. The calculations were symmetrized[35] with respect to the sequence of emission of particles x_1 and x_2.

The predicted correlations are shown by the solid lines in Figs. 8—13. For comparison, the dashed lines show calculations which neglect the effects of energy conservation by using $T=T'$. (The effect of the energy conservation requirement cannot be assessed unambiguously, since it involves assumptions about the relation between excitation energy and temperature.) For each particle combination, the calculated correlation functions were multiplied with a single normalization constant which was chosen to provide reasonable overall agreement with the magnitude of the measured correlations. The calculations reproduce the qualitative trends of the experimental correlations rather well. The enhanced emission of coincident particles to opposite sides of the beam axis and the increasing importance of this effect for heavier particles are well described by both calculations, suggesting the dominance of phase space constraints due to momentum conservation. The effects of energy conservation are, however, not negligible. They are most pronounced for the in-plane

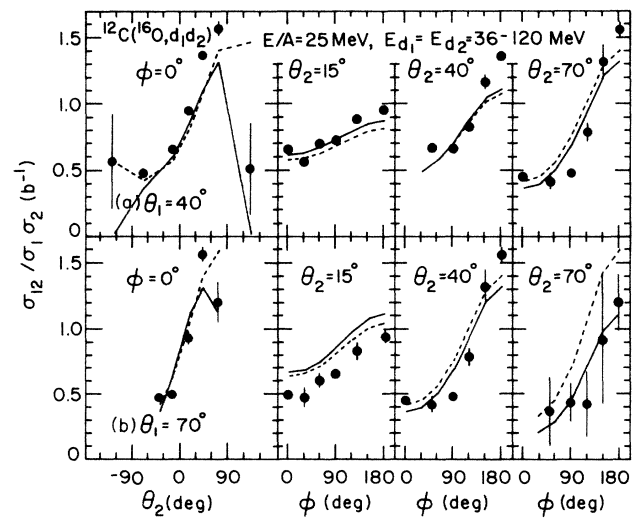

FIG. 11. Two-particle correlations between coincident deuterons emitted in ^{16}O induced reactions on ^{12}C at $E/A=25$ MeV. The solid and dashed lines are explained in the text.

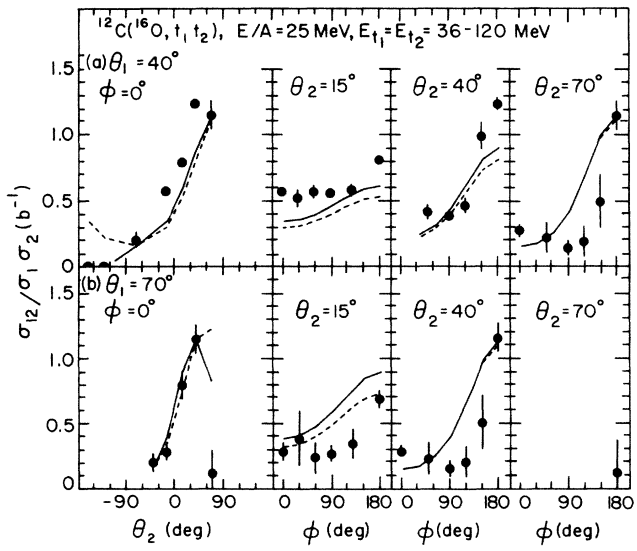

FIG. 13. Two-particle correlations between coincident tritons emitted in ^{16}O induced reactions on ^{12}C at $E/A=25$ MeV. The solid and dashed lines are explained in the text.

correlations at large negative angles θ_2. At these angles, the decreased temperature T' enhances the effect of the motion of the recoiling source, increasing the likelihood for emission to the opposite side of the beam axis.

The detailed shapes of the azimuthal distributions are not reproduced by our schematic calculations. While these assume isotropic emission in the rest frame of the respective source, better agreement with the data could be obtained by including angular momentum effects. Clearly, the detailed shapes of the correlation functions will also be sensitive to the reaction dynamics. Different two-particle correlations may arise for systems which disintegrate instantaneously or via a sequence of statistical decays. In a more microscopic picture, the correlation functions are expected to be sensitive to the effects of the mean field as well as the effects of individual nucleon-nucleon collisions. It is, however, less our purpose to fit the observed correlations with a specific model than to demonstrate with our calculations that momentum and energy conservation dominate the two-particle correlation functions for small nuclear systems. Our discussion should make it clear that meaningful comparisons with specific models can only be made if these models incorporate relevant conservation laws. While present microscopic calculations[27,39,40] with the Boltzmann-Uehling-Uhlenbeck equation make consistent predictions of single particle distributions, they do not incorporate the effects of energy and momentum conservation in such a way that two-particle correlations are fully comparable to the data.[27] Comparisons of two-particle correlations measured for small nuclear systems with these calculations are, therefore, of limited value.

Two-particle correlations measured for the reaction ^{16}O + ^{197}Au are shown in Figs. 14–19. For this heavier system, momentum conservation effects are significantly less pronounced.[17] Consequently, the correlations do not exhibit the pronounced enhancement of coincident particle emission to opposite sides of the beam axis which dominates the correlations measured for the ^{16}O + ^{12}C reaction. The azimuthal correlations are nearly symmetric about the beam axis. They exhibit a minimum at $\phi=90°$ which becomes more pronounced at larger angles, θ_1 and θ_2, and with increasing mass of the emitted particles. The in-plane correlations exhibit a minimum at forward angles; they are peaked at intermediate angles and decrease towards larger polar angles, $|\theta_2| \geqq 90°$.

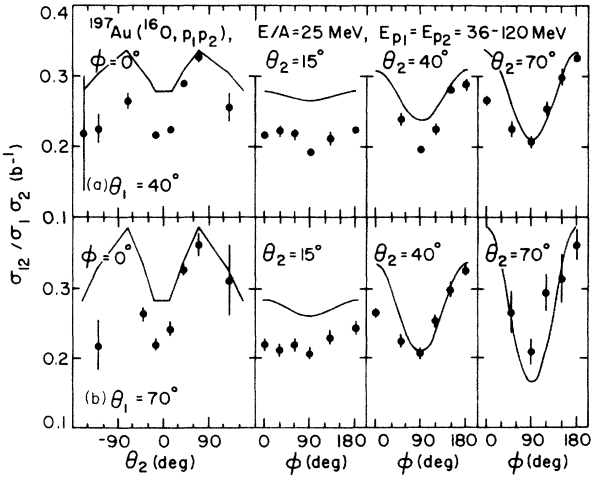

FIG. 14. Two-particle correlations between coincident protons emitted in ^{16}O induced reactions on ^{197}Au at $E/A=25$ MeV. The solid lines are explained in the text.

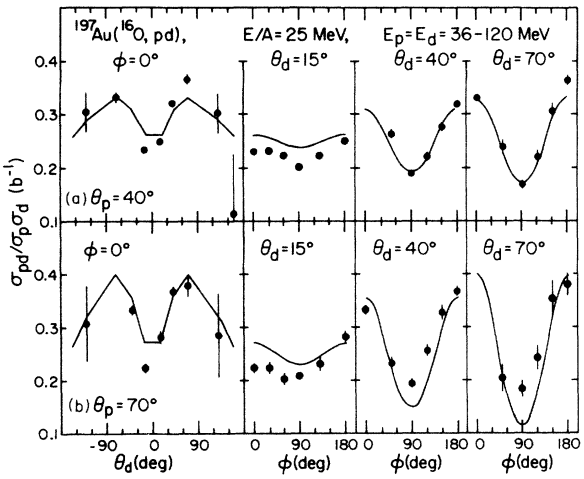

FIG. 15. Two-particle correlations between coincident protons and deuterons emitted in ^{16}O induced reactions on ^{197}Au at $E/A=25$ MeV. The solid lines are explained in the text.

The qualitative features of the two-particle correlations for the ^{16}O + ^{197}Au reaction can be understood in terms of an ordered transverse motion in the entrance channel reaction plane which is superimposed onto the random motion of the individual light particles.[17] In order to illustrate this effect, we performed schematic calculations based on the parametrization of Eq. (5). Neglecting momentum and energy conservation effects, the two-particle coincidence cross section was expressed as[17]

$$\frac{d^4\sigma_{12}}{dE_1 d\Omega_1 dE_2 d\Omega_2}(E_1,E_2,\theta_1,\theta_2,\phi) = \int_0^{2\pi} d\xi \frac{d^2\sigma_1}{dE_1 d\Omega_1}(E_1,\theta_1,\xi)\frac{d^2\sigma_2}{dE_2 d\Omega_2}(E_2,\theta_2,\phi+\xi)\,, \tag{9}$$

where the single particle cross sections, $d^2\sigma_1/dE_1 d\Omega_1$ and $d^2\sigma_2/dE_2 d\Omega_2$, are given by Eq. (5). The calculated correlation functions were then obtained by using Eq. (8). The calculations were performed with the following set of parameters:[17] $T=5.6$ MeV, $v_0=0.09c$, $V_c=10$ MeV, $R\omega=0.1c$. For each particle combination, the calculated correlations were multiplied by a single normalization constant which was chosen to provide reasonable overall agreement with the magnitudes of the measured correlations. The calculations describe the qualitative features of the observed correlations rather well. They reproduce the characteristic "V" shape of the azimuthal correlations and the experimental observation that the minimum at $\phi=90°$ becomes more pronounced at larger angles, θ_1 and θ_2, and with increasing mass of the emitted particles. These dependences are clear from the explicit form of Eq. (5).

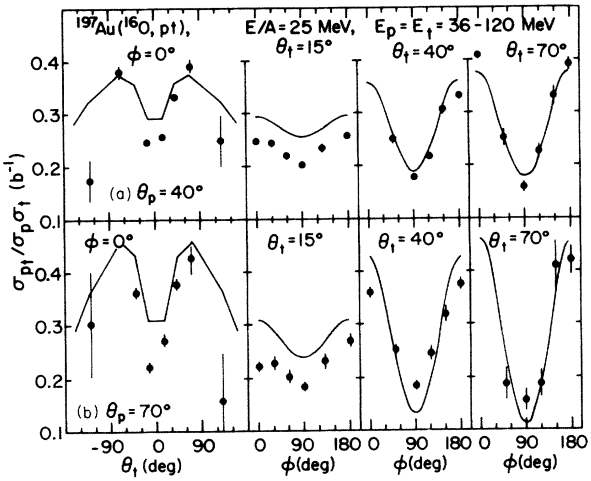

FIG. 16. Two-particle correlations between coincident protons and tritons emitted in ^{16}O induced reactions on ^{197}Au at $E/A=25$ MeV. The solid lines are explained in the text.

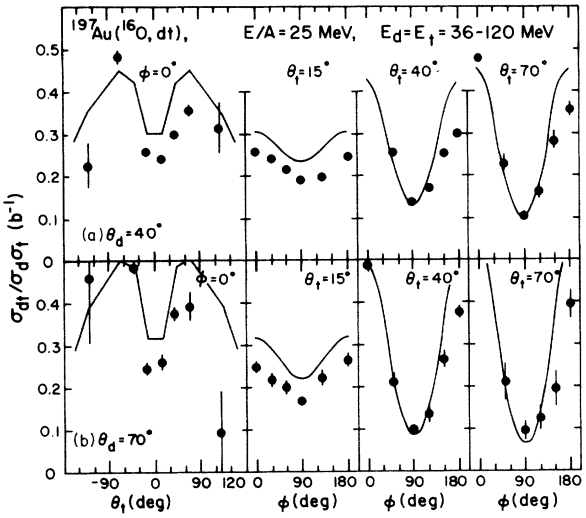

FIG. 18. Two-particle correlations between coincident deuterons and tritons emitted in ^{16}O induced reactions on ^{197}Au at $E/A=25$ MeV. The solid lines are explained in the text.

The mass dependence of the azimuthal correlations may also be understood in terms of simple qualitative arguments. The enhanced coplanar emission of coincident particles may be viewed as due to the superposition of a collective motion (parametrized here in terms of a simple rotation) and a random motion of the individual particles (parametrized here in terms of a temperature). While the velocity component due to the collective motion is independent of the mass of the emitted particles, the thermal velocity component decreases for heavier particles ($v_{\text{thermal}} \propto m^{-1/2}$). The effects due to collective motion are, therefore, more pronounced for heavier particles.

The calculations predict a minimum of the correlation function at small angles, $|\theta_2| \approx 0°$, in qualitative agreement with the experimental in-plane correlations. The occurrence of such a minimum at forward angles is characteristic of systems for which the emission of particles is enhanced in a plane which contains the beam axis.

The depth of the minimum of the in-plane correlation function at small angles is not reproduced by the calculations. It may be possible that additional suppression of the correlation function at small angles is caused by impact parameter averaging effects. Low multiplicity peripheral reactions which do not contribute to the coincidence cross sections can be expected to make increasing contributions to the single particle inclusive cross sections at small angles, resulting in a suppression of the correlation function. To address this question, multiplicity selected, two-particle correlation data are needed.

Close inspection of the coincidence cross sections at $\phi=0°$ and 180° reveals a small enhancement for the emission of coincident protons to opposite sides of the beam axis. Coincident deuterons and tritons, on the other hand, are preferentially emitted to the same side of the beam axis. It is possible that these in-plane asymmetries are the result of the competing effects of momentum conservation and the refractive or absorptive interactions of the outgoing particles with the heavy reaction residue. At

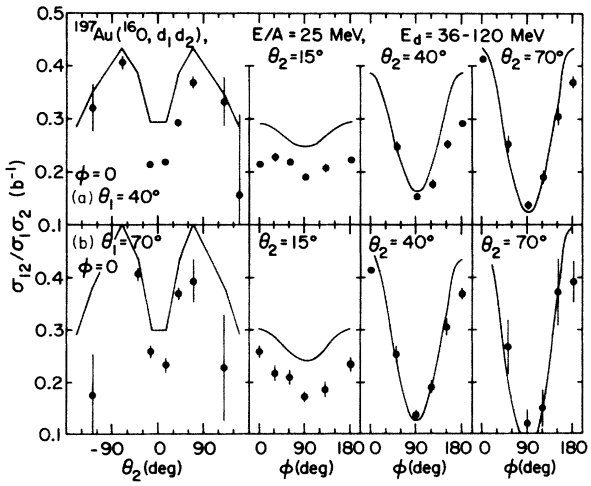

FIG. 17. Two-particle correlations between coincident deuterons emitted in ^{16}O induced reactions on ^{197}Au at $E/A=25$ MeV. The solid lines are explained in the text.

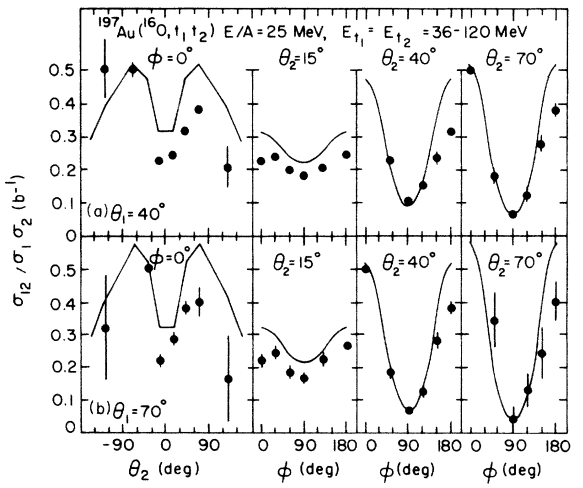

FIG. 19. Two-particle correlations between coincident tritons emitted in ^{16}O induced reactions on ^{197}Au at $E/A=25$ MeV. The solid lines are explained in the text.

small relative angles further complications may result from final state interactions of the emitted particles and from the sequential decays of highly excited primary reaction products.[41,42]

As a final comment, we wish to emphasize that the comparison of the two-particle correlation functions with our schematic parametrizations serves only to elucidate certain general features which must be reproduced by more complete models of noncompound light particle emission. We expect that similar agreement with the measured correlations can be obtained by other models which incorporate the superposition of collective and random velocity components and the phase space constraints caused by energy and momentum conservation.

VI. SUMMARY AND CONCLUSION

We have measured single- and two-particle inclusive cross sections for the emission of protons, deuterons, and tritons, for ^{16}O induced reactions on ^{12}C, ^{27}Al, and ^{197}Au at $E/A=25$ MeV. The single particle inclusive cross sections were shown to follow the systematic trends established for similar reactions and over a wide range of incident energies.[10,14] We have employed several different parametrizations to characterize particle emission at intermediate rapidities. The integrated cross sections extracted with different parametrizations can differ by as much as 30%; relative particle production cross sections can be extracted with better accuracy (typical uncertainties are of the order of 10%).

The two-particle inclusive cross sections exhibit large azimuthal anisotropies. For reactions on ^{12}C, the angular correlations are dominated by the phase space constraints imposed by momentum and energy conservation on small nuclear systems. Since these constraints cannot be evaluated in a model independent fashion, the presence of collective effects mediated by the mean nuclear field cannot be established unambiguously. Comparisons with more microscopic calculations, such as the Boltzmann-Uehling-Uhlenbeck approach,[27,39,40] will only be meaningful once momentum conservation effects are correctly incorporated into the calculations.

For reactions on ^{197}Au, momentum conservation effects are less pronounced. Noncompound light particles are preferentially emitted in a plane which contains the beam axis. Previous coincidence measurements between noncompound light particles and fission fragments indicate that this plane corresponds to the entrance channel scattering plane.[26] The experimental two-particle correlation functions can be described in terms of an ordered motion in this plane which is superimposed onto the random motion of the individual particles. In terms of a more microscopic model, the ordered motion is associated with the propagation of the particles in the mean nuclear field.[27] The random components of the particle velocities are influenced by individual nucleon-nucleon collisions.

We have employed a simple parametrization to simulate the superposition of collective and random velocity components. This parametrization could describe the overall trends of the two-particle correlation functions rather well. It also provided better fits to the single particle inclusive cross sections than simple Maxwellian distributions. Temperature parameters extracted by this parametrization were consistently lower than those extracted from fits with Maxwellian distributions, illustrating that absolute temperature determinations from the slopes of single particle inclusive energy spectra can be associated with considerable uncertainties.

As a final remark, we wish to emphasize that our use of simple model parametrizations ought to be viewed only as an attempt to illustrate some of the main characteristics of the data. A deeper understanding of the underlying physics will have to emerge from microscopic approaches which incorporate the effects mediated by the nuclear mean field, individual nucleon-nucleon collisions, conservation laws, and composite particle formation in a consistent way.

This work was supported jointly by the National Science Foundation under Grant No. PHY 83-12245 and by the U.S. Department of Energy under Contract No. DE-AC05-84OR21400 with Martin Marietta Energy Systems, Inc.

APPENDIX: CLASSICAL PARTICLE EVAPORATION FROM A ROTATING SPHERE

Following the derivation of Halpern,[28] we give a brief discussion of particle evaporation from a rotating sphere of radius R and temperature T assuming a Maxwellian energy distribution in the interior. The flux of particles leaving a surface element dS is proportional to

$$\frac{d^5N}{dt\,dS\,d^3v'} \propto \rho(\mathbf{R})\cdot(\hat{\mathbf{n}}\cdot\mathbf{v}')\exp(-E'/T)\ , \tag{A1}$$

where $\rho(\mathbf{R})$ is the density of particles at the surface, $E'=mv'^2/2$ is the energy of a particle in the interior defined with respect to the rotating reference frame, and $\hat{\mathbf{n}}$ is the unit vector normal to the surface element dS. For a sphere of angular velocity ω, the exterior velocity with respect to the nonrotating external reference frame, $\mathbf{v}$, is given by

$$\mathbf{v}'^2=\mathbf{v}^2+R^2(\hat{\mathbf{n}}\times\boldsymbol{\omega})^2+2R\hat{\mathbf{n}}\cdot(\boldsymbol{\omega}\times\mathbf{v})+2W/m\ , \tag{A2}$$

where W is the difference in potential energy across the surface. (W is assumed to be a constant.) The density of a rotating ideal gas in hydrostatic equilibrium is given by

$$\rho(r)=\rho_0\exp(m\omega^2r^2/2T)\ , \tag{A3}$$

where r denotes the distance from the axis of rotation. At the surface we have $\omega^2r^2=R^2(\hat{\mathbf{n}}\times\boldsymbol{\omega})^2$ and:

$$\rho(\mathbf{R})=\rho_0\exp[mR^2(\hat{\mathbf{n}}\times\boldsymbol{\omega})^2/2T]\ . \tag{A4}$$

Using $\hat{\mathbf{n}}\cdot\mathbf{v}'d^3v'=\hat{\mathbf{n}}\cdot\mathbf{v}d^3v$, one obtains

$$\frac{d^5N}{dt\,dS\,d^3v} \propto (\hat{\mathbf{n}}\cdot\mathbf{v})\exp\{-(m/2T) \times[v^2+2R\hat{\mathbf{n}}\cdot(\boldsymbol{\omega}\times\mathbf{v})]\} \ . \quad \text{(A5)}$$

Choosing a coordinate system (indicated by a subscript 1) with $\mathbf{v}$ parallel to the z axis and $\boldsymbol{\omega}$ in the x-z plane, we have

$$\hat{\mathbf{n}}\cdot(\boldsymbol{\omega}\times\mathbf{v}) = -v\omega\sin\theta_1\sin\phi_1\sin\alpha \ , \quad \text{(A6)}$$

where α is the angle between $\mathbf{v}$ and $\boldsymbol{\omega}$ and $\hat{\mathbf{n}}=\hat{\mathbf{n}}(\theta_1,\phi_1)$. With $dS=R^2d\phi_1 d(\cos\theta_1)$ and $E=mv^2/2$, integration over the surface of the decaying nucleus provides

$$\frac{d^3N}{dt\,dE\,d\Omega} \propto E\exp(-E/T)\int d\Omega_1\cos\theta_1\exp[(2mE)^{1/2}R\omega\sin\phi_1\sin\theta_1\sin\alpha/T]$$
$$\propto E\exp(-E/T)\frac{J_1(iAE^{1/2}\sin\alpha)}{iAE^{1/2}\sin\alpha} \ , \quad \text{(A7)}$$

where $A=(2m)^{1/2}R\omega/T$, and J_1 is the first order Bessel function. Rotation to a coordinate system with the z axis parallel to the beam axis and $\boldsymbol{\omega}$ chosen to be parallel to the y axis yields

$$\sin\alpha=(1-\sin^2\theta\sin^2\phi)^{1/2} \ , \quad \text{(A8)}$$

where θ and ϕ denote the polar and azimuthal angle of the emitted particle. Inserting into (A7) gives

$$\frac{d^3N}{dt\,dE\,d\Omega} \propto E\exp(-E/T) \times\frac{J_1[iA(E-E\sin^2\theta\sin^2\phi)^{1/2}]}{iA(E-E\sin^2\theta\sin^2\phi)^{1/2}} \ . \quad \text{(A9)}$$

Transformation into the laboratory gives Eq. (5) of the text.

*Present address: Areté Associates, P.O. Box 6024-PT, Sherman Oaks, CA 91413.

[1]W. U. Schröder and J. R. Huizenga, *Treatise in Heavy Ion Science*, edited by D. A. Bromley (Plenum, New York, 1984), Vol. 2, p. 115.
[2]J. R. Birkelund and J. R. Huizenga, Annu. Rev. Nucl. Sci. **33**, 265 (1983).
[3]U. Mosel, *Treatise in Heavy-Ion Science*, Ref. 1, Vol. 2, p. 3.
[4]F. Pühlhofer, Nucl. Phys. **A280**, 267 (1977).
[5]R. L. Auble, J. B. Ball, F. E. Bertrand, R. L. Ferguson, C. B. Fulmer, I. Y. Lee, R. L. Robinson, G. R. Young, J. R. Wu, J. C. Wells, and H. Yamda, Phys. Rev. C **25**, 2504 (1982).
[6]R. L. Auble, J. B. Ball, F. E. Bertrand, C. B. Fulmer, D. C. Hensley, I. Y. Lee, R. L. Robinson, P. H. Stelson, D. L. Hendrie, H. D. Holmgren, J. D. Silk, and H. Breuer, Phys. Rev. Lett. **49**, 441 (1982).
[7]J. B. Ball, C. B. Fulmer, M. L. Mallory, and R. L. Robinson, Phys. Rev. Lett. **40**, 1698 (1978).
[8]T. C. Awes, C. K. Gelbke, B. B. Back, A. C. Mignerey, K. L. Wolf, P. Dyer, H. Breuer, and V. E. Viola, Jr., Phys. Lett. **87B**, 43 (1979).
[9]T. C. Awes, G. Poggi, C. K. Gelbke, B. B. Back, B. G. Glagola, H. Breuer, and V. E. Viola, Jr., Phys. Rev. C **24**, 89 (1981).
[10]T. C. Awes, S. Saini, G. Poggi, C. K. Gelbke, D. Cha, R. Legain, and G. D. Westfall, Phys. Rev. C **25**, 2361 (1982).
[11]R. L. Robinson, R. L. Auble, I. Y. Lee, M. J. Martin, G. R. Young, J. Gomez del Campo, J. B. Ball, F. E. Bertrand, R. L. Ferguson, C. B. Fulmer, J. R. Wu, J. C. Wells, and H. Yamada, Phys. Rev. C **24**, 2084 (1981).
[12]R. L. Robinson, R. L. Auble, J. B. Ball, F. E. Bertrand, R. L. Ferguson, C. B. Fulmer, J. Gomez del Campo, I. Y. Lee, R. W. Novotny, G. R. Young, J. C. Wells, C. F. Maguire, and H. Yamada, Phys. Rev. C **27**, 3006 (1983).
[13]M. Fatyga, K. Kwiatkowski, V. E. Viola, C. B. Chitwood, D. J. Fields, C. K. Gelbke, W. G. Lynch, J. Pochodzalla, M. B. Tsang, and M. Blann, Phys. Rev. Lett. **55**, 1376 (1985).
[14]G. D. Westfall, B. V. Jacak, N. Anantaraman, M. W. Curtin, G. M. Crawley, C. K. Gelbke, B. Hasselquist, W. G. Lynch, D. K. Scott, M. B. Tsang, M. J. Murphy, T. J. M. Symons, R. Legrain, and T. J. Majors, Phys. Lett. **116B**, 118 (1982).
[15]G. D. Westfall, Z. M. Koenig, B. V. Jacak, L. H. Harwood, G. M. Crawley, M. W. Curtin, C. K. Gelbke, B. Hasselquist W. G. Lynch, A. D. Panagiotou, D. K. Scott, H. Stöcker, and M. B. Tsang, Phys. Rev. C **29**, 861 (1984).
[16]C. K. Gelbke, Nucl. Phys. **A400**, 473c (1983).
[17]M. B. Tsang, W. G. Lynch, C. B. Chitwood, D. J. Fields, D. R. Klesch, C. K. Gelbke, G. R. Young, T. C. Awes, R. L. Ferguson, F. E. Obenshain, F. Plasil, and R. L. Robinson, Phys. Lett. **148B**, 265 (1984).
[18]W. G. Lynch, C. B. Chitwood, M. B. Tsang, D. J. Fields, D. R. Klesch, C. K. Gelbke, G. R. Young, T. C. Awes, R. L. Ferguson, F. E. Obenshain, F. Plasil, R. L. Robinson, and A. D. Panagiotou, Phys. Rev. Lett. **51**, 1850 (1983).
[19]C. B. Chitwood, J. Aichelin, D. H. Boal, G. Bertsch, D. J. Fields, C. K. Gelbke, W. G. Lynch, M. B. Tsang, J. C. Shillcock, T. C. Awes, R. L. Ferguson, F. E. Obenshain, F. Plasil, R. L. Robinson, and G. R. Young, Phys. Rev. Lett. **54**, 302 (1985).
[20]M. A. Bernstein, W. A. Friedman, W. G. Lynch, C. B. Chitwood, D. J. Fields, C. K. Gelbke, M. B. Tsang, T. C. Awes, R. L. Ferguson, F. E. Obenshain, F. Plasil, R. L. Robinson, and G. R. Young, Phys. Rev. Lett. **54**, 402 (1985).

[21]Nearly identical fits are obtained if one uses relativistic kinematics. The parameters extracted from relativistic and nonrelativistic expressions differ by less than 2%.

[22]This correction neglects the recoil velocity of the target residue and the angular deflections of the emitted particles in the Coulomb field.

[23]G. D. Westfall, J. Gosset, P. J. Johansen, A. M. Poskanzer, W. G. Meyer, H. H. Gutbrod, A. Sandoval, and R. Stock, Phys. Rev. Lett. **37**, 1202 (1976).

[24]J. Gosset, H. H. Gutbrod, W. G. Meyer, A. M. Poskanzer, A. Sandoval, R. Stock, and G. D. Westfall, Phys. Rev. C **16**, 629 (1977).

[25]H. Heckwolf, Ph.D. thesis, University of Marburg, GSI Report 86-3, January 1986, ISSN: 0171-4546.

[26]M. B. Tsang, C. B. Chitwood, D. J. Fields, C. K. Gelbke, D. R. Klesch, W. G. Lynch, K. Kwiatkowski, and V. E. Viola, Jr., Phys. Rev. Lett. **52**, 1967 (1984).

[27]J. Aichelin and G. Bertsch, Phys. Rev. C **31**, 1730 (1985), and private communication.

[28]I. Halpern (unpublished).

[29]A. S. Goldhaber, Phys. Rev. C **17**, 2243 (1978).

[30]P. J. Siemens and J. O. Rasmussen, Phys. Rev. Lett. **42**, 880 (1970).

[31]B. V. Jacak, G. D. Westfall, C. K. Gelbke, L. H. Harwood, W. G. Lynch, D. K. Scott, H. Stöcker, M. B. Tsang, and T. J. M. Symons, Phys. Rev. Lett. **51**, 1846 (1983).

[32]B. V. Jacak, H. Stöcker, and G. D. Westfall, Phys. Rev. C **29**, 1744 (1984).

[33]P. J. Siemens and J. I. Kapusta, Phys. Rev. Lett. **43**, 43 (1979).

[34]L. P. Csernai and J. I. Kapusta, Phys. Rep. **131**, 223 (1986).

[35]W. G. Lynch, L. W. Richardson, M. B. Tsang, R. E. Ellis, and C. K. Gelbke, Phys. Lett. **108B**, 274 (1982).

[36]R. K. Bhowmik, E. C. Pollacco, J. B. A. England, G. C. Morrison, and N. E. Sanderson, Nucl. Phys. **A363**, 516 (1981).

[37]R. K. Bhowmik, J. Van Driel, R. H. Siemssen, G. J. Balster, P. B. Goldhoorn, S. Gonggrijp, Y. Iwasaki, R. V. F. Jannsens, H. Sakai, K. Siwek-Wilczynska, W. A. Sterrenburg, and J. Wilczynski, Nucl. Phys. **A390**, 117 (1982).

[38]T. C. Awes and C. K. Gelbke, Phys. Rev. C **27**, 137 (1983).

[39]G. Bertsch, H. Kruse, and S. Das Gupta, Phys. Rev. C **29**, 673 (1984).

[40]H. Kruse, B. Jacak, and H. Stöcker, Phys. Rev. Lett. **54**, 289 (1985).

[41]J. Pochodzalla, W. A. Friedman, C. K. Gelbke, W. G. Lynch, M. Maier, D. Ardouin, H. Delagrange, H. Doubre, C. Grégoire, A. Kyanowski, W. Mittig, A. Péghaire, J. Péter, F. Saint-Laurent, Y. P. Viyogi, B. Zwieglinski, G. Bizard, F. Lefèbvres, B. Tamain, and J. Québert, Phys. Rev. Lett. **55**, 177 (1985).

[42]J. Pochodzalla, W. A. Friedman, C. K. Gelbke, W. G. Lynch, M. Maier, D. Ardouin, H. Delagrange, H. Doubre, C. Grégoire, A. Kyanowski, W. Mittig, A. Péghaire, J. Péter, F. Saint-Laurent, Y. P. Viyogi, B. Zwieglinski, G. Bizard, F. Lefèbvres, B. Tamain, and J. Québert, Phys. Lett. **161B**, 275 (1985); **161B**, 256 (1985).

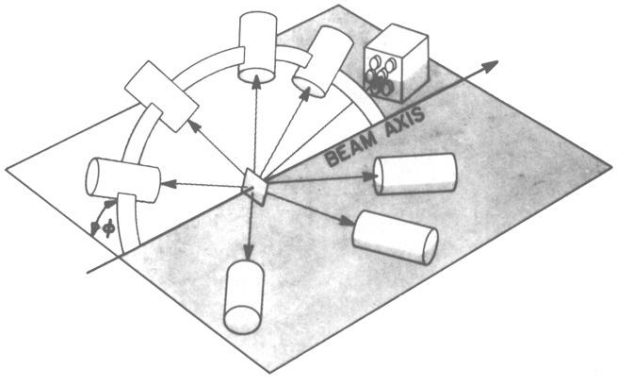

FIG. 1. Schematic diagram of the experimental setup.